Journal of Quantitative Spectroscopy & Radiative Transfer 253 (2020) 107156

Contents lists available at ScienceDirect

Journal of Quantitative Spectroscopy & Radiative Transfer

journal homepage: www.elsevier.com/locate/jqsrt

Hybrid Tamm and surface plasmon polaritons in resonant photonic structure☆

Rashid G. Bikbaev[a,b,*], Stepan Ya Vetrov[b,a], Ivan V. Timofeev[a,b]

[a] L.V. Kirensky Institute of Physics, Federal Research Center KSC SB RAS, 660036, Krasnoyarsk, Russia
[b] Siberian Federal University, 660041, Krasnoyarsk, Russia

ARTICLE INFO

Article history:
Received 11 March 2020
Revised 3 June 2020
Accepted 6 June 2020
Available online 8 June 2020

Keywords:
Tamm plasmon polariton
Surface plasmon polariton
Metal-dielectric nanocomposite
Hybrid mode
Optical sensor

ABSTRACT

Hybrid modes originating from the coupling of the Tamm and surface plasmon polaritons excited in a one-dimensional resonant photonic structure are demonstrated. The structure represents a photonic crystal bounded by a nanocomposite film consisting of a transparent matrix and silver nanoparticles uniformly distributed over its volume. In comparison with structures on planar metal films the volume concentration and shape of nanoparticles are of great help in configuring the hybrid mode properties, including their wavelength and splitting. Also the radiation incidence angle variation opens the possibility of fine-tuning the energy spectra of the structure. We demonstrate the high-sensitivity of optical sensors based on the resonant photonic structure.

1. Introduction

The Tamm plasmon polariton (TPP) is a special type of the interface electromagnetic state. The local field of TPP decays exponentially on each side of the interface. The TPP energy flow along the surface can be completely suppressed at normal excitation [1]. This localized state is analogous to the Tamm electronic state in which the electron density is concentrated at the boundary of a crystal periodic potential [2]. The TPP manifests itself in experiments as a narrow resonance in the optical transmittance or reflectance spectrum of a sample inside the band gap [3,4]. The theoretical and experimental study of the properties of the TPPs offered an opportunity for their use in designing a fundamentally new class of devices, including absorbers [5,6], switches [7], organic solar cells [8–10], thermal emitters [11], sensors [12,13] and filters [14].

Special attention is focused on the TPP hybridization with localized modes of other types. In [15,16], the existence of TPP-exciton hybrid modes was theoretically and experimentally investigated. These modes were obtained by embedding quantum walls near a metallic layer. In this case, the high localization of the field at the TPP wavelength ensures the high-intensity emission of excitons in the quantum walls. By tuning the parameters of the structure, one can change the wavelengths of emission peaks. Close attention is paid to the hybrid modes that originate from the coupling of the TPP with a microcavity (MC) mode. For example, it was shown in [17,18] that the positions of the resonant wavelengths can be tuned by changing the polarization of incident light and forming a structure with an introduced metallic layer of variable thickness and scanning this structure by a light beam of small aperture. In [19], a new design of organic solar cells was proposed, in which the absorption of light was enhanced by means of a broad doubled spectral peak corresponding to the hybrid modes. An idea of light emission at two resonant wavelengths corresponding to the hybrid modes was used for white organic light-emitting diode [20]. Such organic light-emitting diode has a great potential for use in power-efficient light sources and full-color flat panel displays.

In the photonic structures, the TPPs and surface plasmon polaritons (SPPs) can be simultaneously excited [21]. The TPP-SPP hybrid modes were found first in the experiments reported in [22]. It was proposed to use them in sensors sensitive to the refractive index of a material coating a metallic film [23] and enhancing luminescence of molecules placed upon it [24]. Most of the above-mentioned devices are based on one-dimensional photonic crystals conjugated with planar metallic films.

New opportunities are opened up by using structural elements made of resonant materials, e.g., metal-dielectric nanocomposites (NCs). The NC consists of metallic nanoparticles dispersed in a transparent matrix. The NC is characterized by the resonant effective permittivity, whereas the optical characteristics of the initial materials have no resonant features [25,26]. The position of the

☆ Fully documented templates are available in the elsarticle package on http://www.ctan.org/tex-archive/macros/latex/contrib/elsarticle CTAN.

* Corresponding author.
E-mail address: bikbaev@iph.krasn.ru (R.G. Bikbaev).

https://doi.org/10.1016/j.jqsrt.2020.107156
0022-4073/

frequency range where the NC is similar to a metal, i.e., where $\Re\varepsilon_{\text{eff}} < 0$, depends on the permittivities of initial materials, concentration, orientation and shape of nanoparticles, which opens wide possibilities of the control of optical properties of the NC. Currently, there are many methods for producing NC films, such as thermal [27,28] and vacuum [29,30] evaporation, electrodeposition [31], sono- and photochemical approaches [32], electrochemical methods [33], radio frequency sputtering [34], dip coating [35] and spin coating [36]. The spin coating is one of the most attractive deposition methods because of its simple and cheap implementation, its compatibility with other manufacturing processes, and the ability to obtain a uniform thickness of the nanocomposite film [37]. Many of these methods are based on sol-gel technology, which is a versatile and inexpensive method for producing a wide range of metal oxide materials. For example in [38], a new method was proposed for the rapid fabrication of SiO_2 and TiO_2 thin films containing gold nanoparticles using spin coating methods. This method is based on the simultaneous synthesis of both the NC matrix and metal inclusions by a relatively low-temperature baking process. The advantage of this method is the ability to form homogeneous NC films with a higher concentration of nanoparticles and the ability to control it during the formation of NC. This makes it possible to adjust the optical properties of the NC within a wide range. Similar NC materials based on gold and silver nanoparticles have numerous applications in various fields of nanotechnology, such as nonlinear optics [39–41], catalysis [42,43] and sensors [36,44,45]. The possibility of using these resonant media to produce the TPPs was demonstrated in [46–49]. In comparison with the conventional planar metal films a wide variety of opportunities was suggested for optimizing the characteristics of the localized modes and efficient control of a photon energy spectrum, as well as transmittance, reflectance, and absorbance spectra of such structures. Therefore, study of the TPP-SPP hybrid states in photonic structures containing metal-dielectric NCs and prediction of new efficient ways of controlling these states are the important tasks, which are solved in this work.

2. Description of the model

A photonic structure (PhC) under study is a layered medium bounded by a finite NC layer (Fig. 1).

The PhC unit cell consists of silicon dioxide SiO_2 [50] and titanium dioxide TiO_2 [51]. The layer thicknesses were $d_a = 100$ nm and $d_b = 50$ nm, respectively, and the number of layers was $N = 7$. The NC layer with thickness $d_{\text{eff}} = 50$ nm consists of spherical metallic particles uniformly distributed over the dielectric matrix. The permittivity of the medium from which the radiation falls onto the PhC structure is $\varepsilon_a = 2.28$. It should be noted that technology allows to produce NC films with thicknesses down to 40 nm [52] and the diameter of the particles is 10 nm. Thus, even

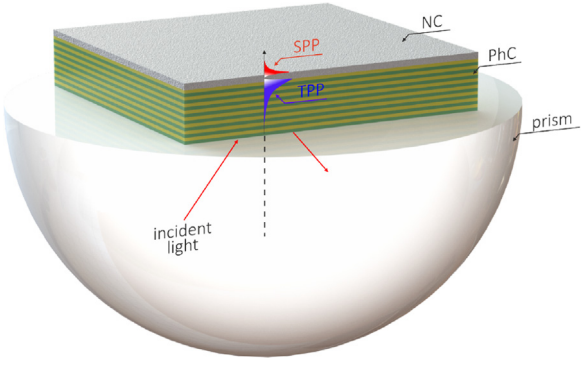

Fig. 1. Schematic of the PhC conjugated with an NC film.

in such thin films, the distribution of nanoparticles over the volume of the NC is uniform. The homogenisation of these media is performed in the volume of the nanocomposite equal to the product of the laser aperture by the thickness of the NC film. This volume contains enough particles to be able to apply the effective medium theory, which is in good agreement with experimental data [38]. In our case the effective permittivity of the NC is determined by the Maxwell-Garnett formula [53] widely used to describe inhomogeneous media. This formula fits a small fraction of isolated metallic inclusions dispersed in the matrix material:

$$\varepsilon_{\text{eff}} = \varepsilon_d \left[1 + \frac{f(\varepsilon_m(\omega) - \varepsilon_d)}{\varepsilon_d + (1-f)(\varepsilon_m(\omega) - \varepsilon_d)L} \right], \tag{1}$$

where f is the filling factor, i.e., the volume fraction of nanoparticles in the matrix; $L = 1/3$ is the factor of depolarization of a sphere; ε_d and $\varepsilon_m(\omega)$ are the permittivities of the matrix and nanoparticle metal, respectively; and ω is the radiation frequency. We find the permittivity of a nanoparticle metal using the Drude approximation

$$\varepsilon_m(\omega) = \varepsilon_0 - \frac{\omega_p^2}{\omega^2 + i\omega\gamma}, \tag{2}$$

where ε_0 is the constant that takes into account the contributions of the interband transitions of bound electrons, ω_p is the plasma frequency, and γ is the reciprocal electron relaxation time. For silver, we have $\varepsilon_0 = 5$, $\hbar\omega_p = 9$ eV, and $\hbar\gamma = 0.02$ eV. The permittivity of the matrix (SCHOTT glass - LaSF, https://refractiveindex.info) is determined as

$$\varepsilon_d = 1 + \frac{2.45505861\lambda^2}{\lambda^2 - 0.0135670404} + \frac{0.453006077\lambda^2}{\lambda^2 - 0.054580302} + \frac{2.3851308\lambda^2}{\lambda^2 - 167.904715}, \tag{3}$$

where λ is the incident radiation wavelength.

In general case the permittivity of the NC can be presented as:

$$\varepsilon_{\text{eff}} = \Re\varepsilon_{\text{eff}} + i\Im\varepsilon_{\text{eff}}. \tag{4}$$

Neglecting the small coefficient γ^2 and using Eqs. (1) and (2), we obtain the resonance wavelength depending on the characteristics of the initial materials and the concentration of the spherical nanoparticles:

$$\lambda_0 = \frac{2\pi c}{\omega_p}\sqrt{\frac{3\varepsilon_d + (1-f)(\varepsilon_0 - \varepsilon_d)}{1-f}}. \tag{5}$$

At the point $\lambda = \lambda_0$, the function $\Re\varepsilon_{\text{eff}}$ vanishes and the function $\Im\varepsilon_{\text{eff}}$ is maximal. The function $\Re\varepsilon_{\text{eff}}$ also vanishes at the point

$$\lambda_1 = \frac{2\pi c}{\omega_p}\sqrt{\frac{\varepsilon_0 + 2\varepsilon_d + 2f(\varepsilon_0 - \varepsilon_d)}{1+2f}}. \tag{6}$$

In the interval $[\lambda_1, \lambda_0]$, the function $\Re\varepsilon_{\text{eff}}$ is negative, $\Re\varepsilon_{\text{eff}} < 0$; i.e., the NC in this frequency range is similar to a metal.

The dependences of the real and imaginary parts of the NC effective permittivity calculated using formula 1 are shown in Fig. 2.

It can be seen that there is a portion where the real part of the permittivity takes negative values; consequently, in this spectral range, the NC exhibits the metallic properties. When the NC metallicity range overlaps with the PhC band gap, a TPP can be excited.

The change in the light field during its passage through the NC-PhC structure is calculated by the transfer matrix method [54,55]. In this method, the state of the field in each structural layer is determined by the second-order transfer matrix and the transfer

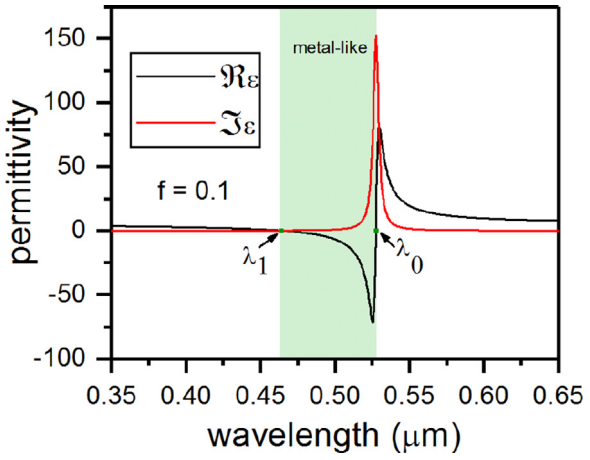

Fig. 2. Dependences of the real and imaginary parts of the NC effective permittivity on the incident radiation wavelength. The filling factor is $f = 0.1$.

matrix of the entire structure, which relates amplitudes of the incident and outgoing waves, is a product of such 2 × 2 matrices:

$$\hat{M} = \hat{T}_{01}\hat{T}_{12}\ldots\hat{T}_{N-1,N}\hat{T}_{N,S}, \tag{7}$$

where the transfer matrix is

$$\hat{T}_{n-1,n} = \frac{1}{2}\begin{pmatrix}(1+h)e^{-i\alpha_n\tau_n} & (1-h)e^{i\alpha_n\tau_n}\\ (1-h)e^{-i\alpha_n\tau_n} & (1+h)e^{i\alpha_n\tau_n}\end{pmatrix}. \tag{8}$$

Here for TE-wave, $h = \sqrt{\varepsilon_n - \sin^2\theta}/\sqrt{\varepsilon_{n-1} - \sin^2\theta}$, ε_n is the permittivity of the n-th layer, $\alpha_n = (\omega/c)\sqrt{\varepsilon_n - \sin^2\theta}$, ω is the wave frequency, c is the speed of light, τ_n=z_n–z_{n-1}, n=1,2,...,N are the layer thicknesses, z_n is the coordinate of the interface between the n-th layer and the n+1 layer adjacent from the right, and τ_{N+1} = 0, θ is the angle of light incidence. The transfer matrix for the orthogonally polarized TM-wave is obtained from (8) replacing h by new expression $h' = \varepsilon_{n-1}\sqrt{\varepsilon_n - \sin^2\theta}/\varepsilon_n\sqrt{\varepsilon_{n-1} - \sin^2\theta}$.

The energy transmittances, reflectances, and absorbances are expressed as

$$T(\omega) = \frac{1}{|\hat{M}_{11}|^2}, R(\omega) = \frac{|\hat{M}_{21}|^2}{|\hat{M}_{11}|^2}, \tag{9}$$

$$A(\omega) = 1 - T(\omega) - R(\omega).$$

where $\hat{M}_{11}$ and $\hat{M}_{21}$ are the elements of the matrix $\hat{M}$.

3. Results

Fig. 3 shows the reflectance spectra of the structure for the TM-waves calculated by the transfer matrix method at different filling factors f and angles θ of incidence of the radiation onto the structure.

It can be seen that, at the angles of incidence smaller than the angle of total internal reflection ($\theta = 42^o$), which is independent of the factor f, only the TPP is observed in the PhC band gap. At the angles larger than the angle of total internal reflection, the SPP is excited at the NC-air interface. At the specified f values and angles of incidence ($43^o < \theta < 45^o$), the TPP and SPP are coupled and a TPP-SPP hybrid mode can be excited. In the reflectance spectrum, the coupling between two modes can be seen as a splitting of the spectral lines. The splitting value characterizes the mode coupling that can be controlled by changing the NC filling factor. For example, at $f = 0.2$ (Fig. 3d), the splitting is 10 nm; at $f = 0.3$ (Fig. 3f), 18.5 nm; and, at $f \leq 0.1$ (Fig. 3a, b), it is not observed. It is important to note that the absence of splitting does not mean that hybrid modes are not excited. They are formed, but their spectral positions becomes so close to each other that they merge into one broad line. The broadening of the spectral line due to the interaction of the TPP and SPP lines can be used to form a wider absorption band inside the PhC band gap. Much attention is paid to such methods of controlling the energy spectra of the structure, which is due to the possibility of their application in promising areas, e.g. photovoltaics.

It is noteworthy that the TPP and SPP dispersion curves intersect also in the range of $50^o < \theta < 60^o$. Thus, changing the NC

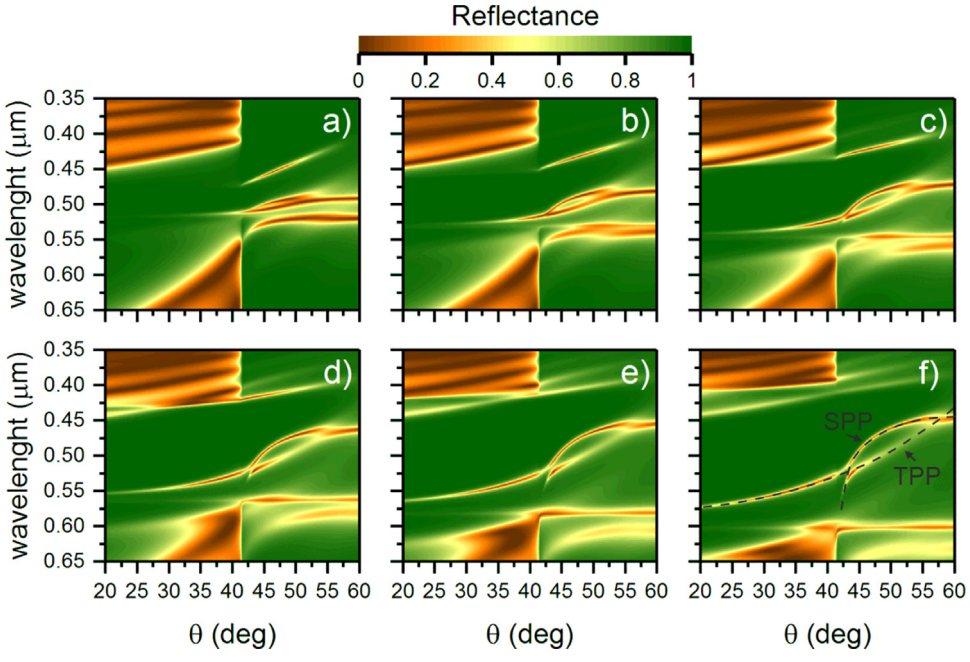

Fig. 3. Reflectance spectra for the PhC conjugated with the NC layer at different angles of incidence of the TM-waves. The NC layer thickness is $d_{eff} = 50$ nm and the frequencies are (a)$f = 0.05$, (b) $f = 0.1$, (c) $f = 0.15$, (d) $f = 0.2$, (e) $f = 0.25$, and (f) $f = 0.30$. Dotted lines show the TPP and SPP spectral positions.

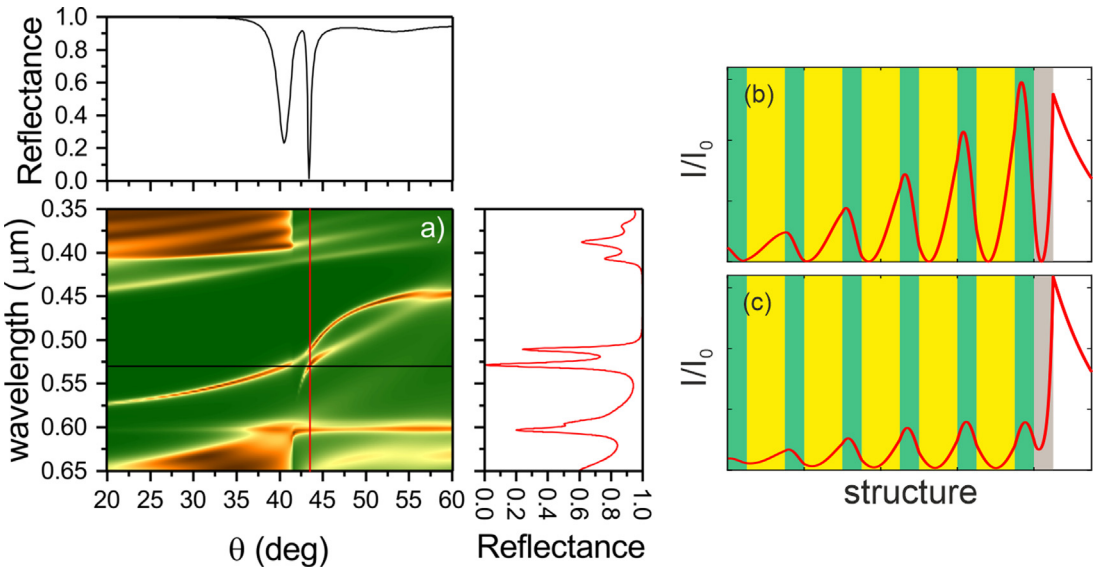

Fig. 4. (a) Reflectance spectra of the PhC conjugated with the NC layer at different angles of incidence of the TM-waves. (b,c) Schematic of a one-dimensional PhC conjugated with the NC layer and field intensity distribution at the hybrid mode wavelengths normalized to the input intensity. The NC layer thickness is $d_{\text{eff}} = 50$ nm, $f = 0.3$.

filling factor and the angle of incidence of the radiation onto the structure, one can create the TPP-SPP hybrid modes in different spectral ranges. The possibility of the frequency detuning of the spectrum by changing the angle of incidence and wavelength of the radiation at a fixed value of $f = 0.3$ is illustrated in Fig. 4a. When the λ value is constant, the change in the angle of incidence makes it possible to switch the TPP to the SPP and backward, since, in this case, they are uncoupled. Thus, it becomes possible to control the spatial distribution of the field in the bulk of the PhC, since, for the TPP, the field is localized at the PhC-NC interface and, for the SPP, at the NC-air interface.

The spectral picture is different at the fixed θ value and variable λ value. For example, at $\theta = 43.5^o$, the TPP and SPP are hybridized. As a result, two reflectance minima are observed at wavelengths of $\lambda = 528.6$ nm and $\lambda = 510.8$ nm in the PhC band gap. The electric field intensity distributions at the corresponding wavelengths are shown in Fig. 4b and c. It can be seen that the field is distributed between two coupled modes and localized at both the PhC-NC and NC-air interfaces. It should be noted, that the values of field localization at the PhC-NC boundaries at $\lambda = 510.8$ nm are less than at the NC-air boundaries. This effect is explained by the fact that at $\lambda = 510.8$ nm, the critical coupling condition of the incident field with the TPP is not fulfilled and, as a result, the weaker field localization is observed.

It should be noted that the field is localized in the region comparable with the wavelength. Such a control of the local field value in the bulk of the PhC upon variation in the angle of incidence and wavelength of the radiation makes these structures promising for use in tunable absorbers and optical switches.

The qualitatively new possibilities for controlling the spectral properties of hybrid modes are opened by changing the shape of nanoparticles dispersed in a transparent matrix. It should be noted, that the anisotropic NC can be obtained by irradiation of the spherical-like metallic nanoparticles by Si ions [56]. This method allows controlling the optical axis of the NC and obtaining elongated particles (10-15 nm) with a small aspect ratio. In this case, the change in the ratio between lengths of the nanoparticle polar and equatorial axes significantly affects the effective permittivity of the NC. This effect can be taken into account by adding formula (1) with the spheroid depolarization factors $L_{\parallel,\perp}$, which depend on the ratio between the lengths of the polar (a) and equatorial (b) spheroid semiaxes and on the field direction [57]. For the field directed along the spheroid axis of rotation, the factor $L_{\parallel}$ is expressed as

$$L_{\parallel} = \frac{1}{1-\xi^2}\left[1 - \xi\frac{\arcsin\sqrt{1-\xi^2}}{\sqrt{1-\xi^2}}\right] \tag{10}$$

and, for the field directed perpendicular to the spheroid axis of rotation,

$$L_{\perp} = \frac{1 - L_{\parallel}}{2}, \tag{11}$$

where $\xi = a/b$. The case $\xi < 1$ corresponds to the oblate spheroid and $\xi > 1$, to the prolate spheroid.

For oblique incidence of light we have to use both $\varepsilon_{\text{eff}_{\parallel}}$ and $\varepsilon_{\text{eff}_{\perp}}$ for definition of effective permittivity of the NC layer. The dependences of the effective permittivity of the NC on ξ value and wavelength of the incident radiation are presented in Fig. 5a. It can be seen in figure that the nanoparticle shape allows one to control the position of the NC resonance and the region of its metallicity ($\Re\varepsilon_{\text{eff}} < 0$). In particular, for prolate and oblate spheroids the NC is similar to a metal only in short wavelength region. The possibility of controlling the properties of the hybrid modes excited in the structure anisotropic NC-PhC is illustrated in 5 b. The change in the parameter ξ not only makes it possible to govern the splitting of the hybrid modes, but also offers an opportunity for their formation. In the range of $1 < \xi < 1.25$, the TPP-SPP hybrid modes are excited, while beyond this range the coupling of these modes is not observed.

The model proposed here can be used for an optical sensor based on the TPP and SPP modes. It should be noted that the sensors based on the TPP-SPP hybrid modes were proposed earlier in [23,58], but their sensitivity was determined by the splitting of the hybrid modes. If losses increase in the structure, the spectral lines are broadened. Corresponding merge of lines obscures sensitivity of an optical sensor, since, in the region of avoided crossing, the Rayleigh criterion should be valid. In view of the aforesaid, we propose another implementation of the optical sensor based on the TPP and SPP. Robust measurement requires a reference line with stable wavelength, weakly dependant on the refractive index of the environment. In our structure, the TPP can be used as a reference line, since its wavelength is independent of the refractive index of

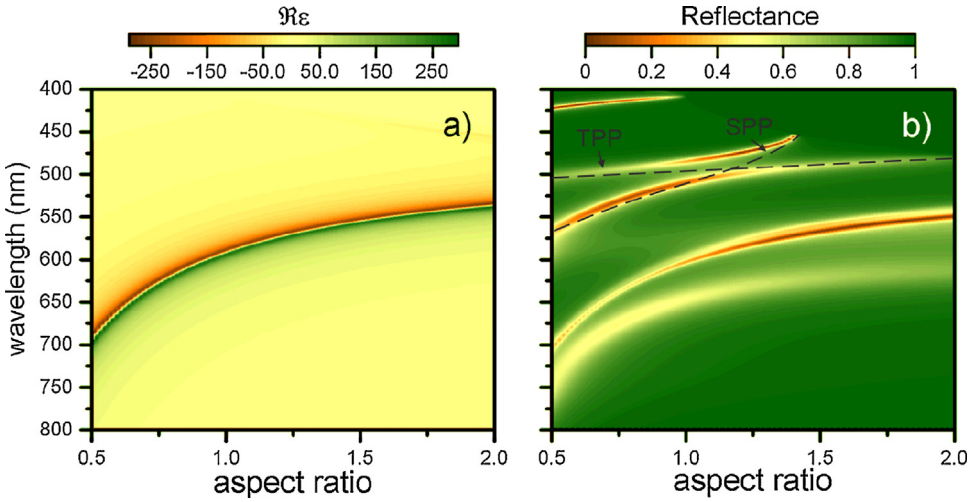

Fig. 5. (a) Dependence of the real part of the effective permittivity of the NC on the wavelength of the incident radiation and ratio between the length of the polar axis of the nanospheroid and the length of its equatorial axis ξ. (b) Reflectance spectra of the PhC conjugated with the anisotropic NC layer at different ξ values and a constant angle of incidence of $\theta = 43.5^o$. The NC layer thickness is $d_{\text{eff}} = 50$ nm, $f = 0.30$.

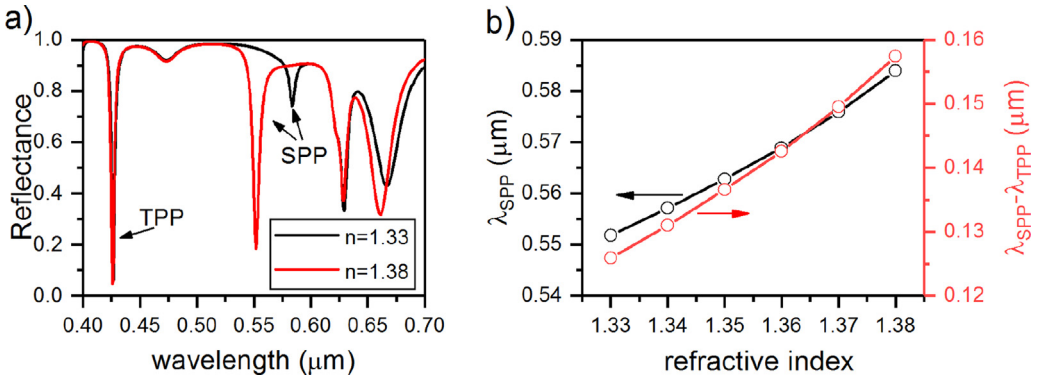

Fig. 6. (a) Reflectance spectra of the structure anisotropic NC-PhC at different refractive indices of the medium above the NC layer and (b) dependencies of the λ_{SPP} and $\Delta\lambda$ on the refractive index of the medium above the NC layer. $\xi = 0.8$, $\theta = 70^o$, $d_{\text{eff}} = 50$ nm, and $f = 0.30$. The thicknesses of PhC layers are $d_a = 130$ nm and $d_b = 60$ nm. The thickness of the TiO_2 layer adjacent to the NC film $d_{\text{top}} = 40$ nm.

the medium above the NC layer. Then, the sensitivity of the sensor will be determined by the shift of the SPP line relative to the TPP line (Fig. 6).

It can be seen in Fig. 6a that the change in the refractive index of the medium above the NC layer leads to the significant variation in the reflectance spectra of the structure under study. In particular, at $n = 1.33$, the wavelengths are $\lambda_{TPP} = 425.9$ nm and $\lambda_{SPP} = 551.8$ nm, while at $n = 1.38$, the wavelengths are $\lambda_{TPP} = 426.5$ nm and $\lambda_{SPP} = 583.9$ nm. The wavelength differences $\Delta\lambda_{n=1.33}$ and $\Delta\lambda_{n=1.38}$ are 125.9 nm and 157.4 nm, respectively (see. Fig. 6b). The spectral sensitivity of the sensor is determined as $S = \Delta\lambda/\Delta n$. At the considered parameter set, this quantity is $S = (\Delta\lambda_{n=1.38} - \Delta\lambda_{n=1.33})/\Delta n = 630$, which is a good sensitivity for the one-dimensional planar structure.

4. Conclusions

The TPP-SPP hybrid modes localized in a resonant photonic structure were investigated. The examined resonant material was a metal-dielectric nanocomposite consisting of a transparent matrix and silver nanoparticles dispersed over its volume. In contrast to the classical metal-PhC system, the proposed model has a great number of degrees of freedom (the volume concentration of nanoparticles and their shape), which allows one to implement the finer spectral tuning of the structure. It was shown that the change in the volume concentration of nanoparticles makes it possible to govern the splitting of hybrid modes and the change in their shape allows one to control the strength of their coupling. This structure with two types of localized modes was proposed to act as optical sensor. In this case we consider non-coupling regime of these modes in which we measure the distance between the TPP and SPP wavelengths upon variation in the refractive index of the medium above the NC layer. It is important to note that in contrast to the previously proposed models, in which the sensitivity was determined by splitting hybrid modes, in our model, the TPP is used as a reference line. This approach allows to measure the distance between two high resolution lines, which can provide higher accuracy and sensitivity of the device. It was demonstrated that the sensitivity of the proposed sensor is $S > 600$ nm/RIU, which is a very good result for device based on TPP or SPP localized in one-dimensional photonic crystal structure.

Funding

The reported study was funded by Russian Foundation for Basic Research, Government of Krasnoyarsk Territory, Krasnoyarsk Region Science and Technology Support Fund to the research project No. 19-42-240004 and by a joint project of the Russian Foundation for Basic Research, project No. 19-52-52006, and the Taiwan Ministry of Science and Technology, project No. 108-2923E-009-003-MY3.

Declaration of Competing Interest

The authors declare that they have no known competing financial interests or personal relationships that could have appeared to influence the work reported in this paper.

References

[1] Kaliteevski MA, Iorsh I, Brand S, Abram RA, Chamberlain JM, Kavokin AV, et al. Tamm plasmon-polaritons: possible electromagnetic states at the interface of a metal and a dielectric bragg mirror. Phys Rev B 2007;76(16):165415. doi:10.1103/PhysRevB.76.165415.

[2] Tamm IE. Phys Z Sowjetunion 1932;1:733.

[3] Sasin ME, Seisyan RP, Kaliteevski MA, Brand S, Abram RA, Chamberlain JM, et al. Tamm plasmon polaritons: slow and spatially compact light. Appl Phys Lett 2008;92(25):251112. doi:10.1063/1.2952486.

[4] Goto T, Dorofeenko AV, Merzlikin AM, Baryshev AV, Vinogradov AP, Inoue M, et al. Optical Tamm states in one-dimensional magnetophotonic structures. Phys Rev Lett 2008;101(11):14–16. doi:10.1103/PhysRevLett.101.113902.

[5] Gong Y, Liu X, Wang L, Lu H, Wang G. Multiple responses of TPP-assisted near-perfect absorption in metal/fibonacci quasiperiodic photonic crystal. Opt Express 2011;19(10):9759. doi:10.1364/OE.19.009759.

[6] Lu G, Wu F, Zheng M, Chen C, Zhou X, Diao C, et al. Perfect optical absorbers in a wide range of incidence by photonic heterostructures containing layered hyperbolic metamaterials. Opt Express 2019;27(4):5326–36. doi:10.1364/OE.27.005326.

[7] Zhang W, Yu S. Bistable switching using an optical Tamm cavity with a Kerr medium. Opt Commun 2010;283(12):2622–6. doi:10.1016/j.optcom.2010.02.035.

[8] Zhang X-L, Song J-F, Li X-B, Feng J, Sun H-B. Optical Tamm states enhanced broad-band absorption of organic solar cells. Appl Phys Lett 2012;101(24):243901. doi:10.1063/1.4770316.

[9] Bikbaev R.G., Vetrov S.Y., Timofeev I.V., Shabanov V.F.. Photosensitivity and reflectivity of the active layer in Tamm plasmon polariton based organic solar cell. 2020.

[10] Zhang X-L, Song J-F, Li X-B, Feng J, Sun H-B. Light trapping schemes in organic solar cells: acomparison between optical Tamm states and Fabry Pérot cavity modes. Org Electron 2013;14(6):1577–85. doi:10.1016/J.ORGEL.2013.03.029.

[11] Yang Z-Y, Ishii S, Yokoyama T, Dao TD, Sun M-G, Pankin PS, et al. Narrowband wavelength selective thermal emitters by confined tamm plasmon polaritons. ACS Photonics 2017;4(9):2212–19. doi:10.1021/acsphotonics.7b00408.

[12] Huang S-G, Chen K-P, Jeng S-C. Phase sensitive sensor on Tamm plasmon devices. Opt Mater Express 2017;7(4):1267. doi:10.1364/OME.7.001267.

[13] Maji PS, Shukla MK, Das R. Blood component detection based on miniaturized self-referenced hybrid tamm-plasmon-polariton sensor. Sens Actuators B 2018;255:729–34. doi:10.1016/j.snb.2017.08.031.

[14] Wu F, Wu J, Fan C, Guo Z, Xue C, Jiang H, et al. Omnidirectional optical filtering based on two kinds of photonic band gaps with different angle-dependent properties. EPL (Europhys Lett) 2020;129(3):34004. doi:10.1209/0295-5075/129/34004.

[15] Kavokin A, Shelykh I, Malpuech G. Optical Tamm states for the fabrication of polariton lasers. Appl Phys Lett 2005;87(26):261105. doi:10.1063/1.2136414.

[16] Symonds C, Lemaître A, Homeyer E, Plenet JC, Bellessa J. Emission of Tamm plasmon/exciton polaritons. Appl Phys Lett 2009;95(15):151114. doi:10.1063/1.3251073.

[17] Brückner R, Sudzius M, Hintschich SI, Fröb H, Lyssenko VG, Leo K. Hybrid optical Tamm states in a planar dielectric microcavity. Phys Rev B 2011;83(3):33405. doi:10.1103/PhysRevB.83.033405.

[18] Brückner R.. Coherence and coupling of cavity photons and Tamm plasmons in metal-organic microcavities2012;:1–135.

[19] Zhang X-L, Song JF, Li XB, Feng J, Sun HB. Strongly localized evanescent optical Tamm states at metal-DBR interface. J Lightwave Technol 2013;31(10):1654–9. doi:10.1109/JLT.2013.2255583.

[20] Zhang X-L, Feng J, Han X-C, Liu Y-F, Chen Q-D, Song J-F, et al. Hybrid Tamm plasmon-polariton/microcavity modes for white top-emitting organic light-emitting devices. Optica 2015;2(6):579. doi:10.1364/OPTICA.2.000579.

[21] Baryshev AV, Kawasaki K, Lim PB, Inoue M. Interplay of surface resonances in one-dimensional plasmonic magnetophotonic crystal slabs. Phys Rev B 2012;85(20). doi:10.1103/physrevb.85.205130.

[22] Afinogenov BI, Bessonov VO, Nikulin AA, Fedyanin AA. Observation of hybrid state of Tamm and surface plasmon-polaritons in one-dimensional photonic crystals. Appl Phys Lett 2013;103(6):61112. doi:10.1063/1.4817999.

[23] Das R, Srivastava T, Jha R. Tamm-plasmon and surface-plasmon hybrid-mode based refractometry in photonic bandgap structures. Opt Lett 2014;39(4):896–9. doi:10.1364/OL.39.000896.

[24] Chen Y, Zhang D, Zhu L, Wang R, Wang P, Ming H, et al. Tamm plasmon- and surface plasmon-coupled emission from hybrid plasmonic–photonic structures. Optica 2014;1(6):407. doi:10.1364/optica.1.000407.

[25] Oraevsky AN, Protsenko IE. Optical properties of heterogeneous media. Quantum Elec (Woodbury) 2001;31(3):252–6. doi:10.1070/QE2001v031n03ABEH001927.

[26] Moiseev SG, Ostatochnikov VA, Sementsov DI. Defect mode suppression in a photonic crystal structure with a resonance nanocomposite layer. Quantum Elec (Woodbury) 2012;42(6):557–60. doi:10.1070/QE2012v042n06ABEH014822.

[27] Pillai S, Catchpole KR, Trupke T, Green MA. Surface plasmon enhanced silicon solar cells. J Appl Phys 2007;101(9):93105. doi:10.1063/1.2734885.

[28] Nakayama K, Tanabe K, Atwater HA. Plasmonic nanoparticle enhanced light absorption in GaAs solar cells. Appl Phys Lett 2008;93(12):121904. doi:10.1063/1.2988288.

[29] Niklasson GA, Brantervik K. Low-frequency dielectric properties of Co-Al2O3 composite films. Appl Phys Lett 1987;50(14):937–9. doi:10.1063/1.97986.

[30] Niklasson GA, Granqvist CG. Dielectric function of coevaporated Co-Al2O3 cermet films. Appl Phys Lett 1982;41(8):773–5. doi:10.1063/1.93673.

[31] Pérez MD, Otal E, Bilmes SA, Soler-Illia GJAA, Crepaldi EL, Grosso D, et al. Growth of gold nanoparticle arrays in TiO2 mesoporous matrixes. Langmuir 2004;20(16):6879–86. doi:10.1021/la0497898.

[32] Yu JC, Wang X-C, Wu L, Ho W-K, Zhang L-Z, Zhou G-T. Sono- and photochemical routes for the formation of highly dispersed gold nanoclusters in mesoporous titania films. Adv Funct Mater 2004;14(12):1178–83. doi:10.1002/adfm.200305145.

[33] Song J-K, Lee U-H, Lee H-R, Suh M, Kwon Y-U. Goldtitania nanocomposite films with a periodic 3D nanostructure. Thin Solid Films 2009;517(19):5705–9. doi:10.1016/j.tsf.2009.02.128.

[34] Armelao L, Barreca D, Bottaro G, Gasparotto A, Tondello E, Ferroni M, et al. Au/TiO2 nanosystems: a Combined RF-Sputtering/sol-Gel approach. Chem Mater 2004;16(17):3331–8. doi:10.1021/cm0353308.

[35] Zhang Y, Yuwono AH, Li J, Wang J. Highly dispersed gold nanoparticles assembled in mesoporous titania films of cubic configuration. Microporous Mesoporous Mater 2008;110(2):242–9. doi:10.1016/j.micromeso.2007.06.009.

[36] Buso D, Post M, Cantalini C, Mulvaney P, Martucci A. Gold nanoparticle-Doped TiO 2 semiconductor thin films: gas sensing properties. Adv Funct Mater 2008;18(23):3843–9. doi:10.1002/adfm.200800864.

[37] Bornside DE, Macosko CW, Scriven LE. Modeling of spin coating. JImaging Technol 1987;13(4):122–30.

[38] Pedrueza E, Valdés JL, Chirvony V, Abargues R, Hernández-Saz J, Herrera M, et al. Novel method of preparation of gold-Nanoparticle-Doped TiO2 and SiO2 plasmonic thin films: optical characterization and comparison with maxwell-Garnett modeling. Adv Funct Mater 2011;21(18):3502–7. doi:10.1002/adfm.201101020.

[39] Cui F, Hua Z, He Q, Li J, Guo L, Cui X, et al. Preparation and third-order optical nonlinearity of gold nanoparticles incorporated mesoporous TiO2 thin films. J Opt Soc Am B 2009;26(1):107. doi:10.1364/JOSAB.26.000107.

[40] Sakhno O, Yezhov P, Hryn V, Rudenko V, Smirnova T. Optical and nonlinear properties of photonic polymer nanocomposites and holographic gratings modified with noble metal nanoparticles. Polymers (Basel) 2020;12(2). doi:10.3390/polym12020480.

[41] Rangel-Rojo R, Sánchez-Esquivel H, Can-Uc B, Crespo-Sosa A, Oliver A. Nonlinear optics with metal-dielectric nanocomposites. Metal Nanostruct Photonics 2019:39–60. doi:10.1016/B978-0-08-102378-5.00003-9.

[42] Idakiev V, Tabakova T, Yuan Z-Y, Su B-L. Gold catalysts supported on mesoporous titania for low-temperature water-gas shift reaction. Appl Catal A 2004;270(1–2):135–41. doi:10.1016/j.apcata.2004.04.030.

[43] Rebrov EV, Berenguer-Murcia A, Johnson BFG, Schouten JC. Gold supported on mesoporous titania thin films for application in microstructured reactors in low-temperature water-gas shift reaction. Catal Today 2008;138(3–4):210–15. doi:10.1016/j.cattod.2008.06.029.

[44] Gradess R, Abargues R, Habbou A, Canet-Ferrer J, Pedrueza E, Russell A, et al. Localized surface plasmon resonance sensor based on Ag-PVA nanocomposite thin films. J Mater Chem 2009;19(48):9233–40. doi:10.1039/b910020b.

[45] Yeshchenko OA, Malynych SZ, Polomarev SO, Galabura Y, Chumanov G, Luzinov I. Towards sensor applications of a polymer/ag nanoparticle nanocomposite film. RSC Adv 2019;9(15):8498–506. doi:10.1039/c9ra00498j.

[46] Vetrov SY, Bikbaev RG, Timofeev I. Optical Tamm states at the interface between a photonic crystal and a nanocomposite with resonance dispersion. J Exp Theor Phys 2013;117(6):988–98. doi:10.1134/S1063776113140185.

[47] Vetrov SY, Bikbaev RG, Timofeev I. The optical Tamm states at the edges of a photonic crystal bounded by one or two layers of a strongly anisotropic nanocomposite. Opt Commun 2017;395:275–81. doi:10.1016/j.optcom.2016.08.075.

[48] Vetrov SY, Bikbaev RG, Rudakova NV, Chen K-p, Timofeev I. Optical Tamm states at the interface between a photonic crystal and an epsilon-near-zero nanocomposite. J Opt 2017;19(8):85103. doi:10.1088/2040-8986/aa75fb.

[49] Vetrov SY, Pankin PS, Timofeev I. The optical Tamm states at the interface between a photonic crystal and a nanocomposite containing coreshell particles. J Opt 2016;18(6):65106. doi:10.1088/2040-8978/18/6/065106.

[50] Malitson IH. Interspecimen comparison of the refractive index of fused silica,. J Opt Soc Am 1965;55(10):1205–9. doi:10.1364/JOSA.55.001205.

[51] DeVore JR. Refractive indices of rutile and sphalerite. J Opt Soc Am 1951;41(6):416–19. doi:10.1364/JOSA.41.000416.

[52] Zhang N, Liu K, Song H, Liu Z, Ji D, Zeng X, et al. Refractive index engineering of metal-dielectric nanocomposite thin films for optical super absorber. Appl Phys Lett 2014;104(20). doi:10.1063/1.4879829.

[53] Maxwell-Garnett JC. Colours in metal glasses, in metallic films, and in metallic solutions. II. Philos R Soc Lond 1906;205:237–88.

[54] Yeh P. Electromagnetic propagation in birefringent layered media. J Opt Soc Am 1979;69(5):742. doi:10.1364/JOSA.69.000742.
[55] Vetrov SY, Pankin PS, Timofeev IV. Peculiarities of spectral properties of a one-dimensional photonic crystal with an anisotropic defect layer of the nanocomposite with resonant dispersion. Quantum Elec (Woodbury) 2014;44(9):881–4. doi:10.1070/qe2014v044n09abeh015473.
[56] Reyes-Esqueda JA, Rodríguez-Iglesias V, Silva-Pereyra H-G, Torres-Torres C, Santiago-Ramírez A-L, Carlos Cheang-Wong J, et al. Nonlinear optics; (190.7070) Two-wave mixing; (190.7110) Ultrafast nonlinear optics; (190.4720) Optical nonlinearities of condensed matter; (160.1190) Anisotropic optical materials Tech. Rep.; 2009.
[57] Golovan LA, Timoshenko VY, Kashkarov PK. Phys Usp 2007;50(6):595. doi:10.1070/pu2007v050n06abeh006257.
[58] Das R, Srivastava T, Jha R. On the performance of Tamm-plasmon and surface-plasmon hybrid-mode refractive-index sensor in metallo-dielectric heterostructure configuration. Sens Actuators B 2015;206:443–8. doi:10.1016/j.snb.2014.09.032.